BioImaging
UCL/BioImaging/Wesely(18057603)
Advance Access Publication Date: 23 April 2019
Applications Note

Respiratory Motion Modelling

Oliver Wesely (18057603) [1]

[1] Department of Computer Science, University College London, London, WC1E 6BT, Great Britain.

Abstract

Motivation: Imaging technology have recently opened up an increasingly wide range of potential applications for medical images. However, in the thorax and abdomen the problem of organ motion caused by respiration remains a limiting factor which we will look at in more details within this paper. Numerous solutions to this problem haven been proposed, while this paper tries to model respiratory motion using sagittal cine-MR images combining various surrogate signals, including the Anterior-Posterior skin signals in the area of abdomen and chest and a Superior-Inferior signal measured by the up and down movement of the diaphragm.
Results: The two best models we found just slightly differ of each other in the results, whereas the first has the lowest overall AIC, the other one has the lowest overall BIC. The first model uses a linear combination of all three surrogate signals mentioned in the abstract, although the slightly better other model actually separates the diaphragm surrogate signal into the inhalation and exhalation corresponding data and fits two separate linear models which we will analysis in more detail.

Contact: oliver.wesely.18@ucl.ac.uk

1 Introduction

Respiratory motion causes problems for many image acquisitions and image guided interventions in the thorax and abdomen. It can cause artefacts and degrade the quality of reconstructed images, and it can cause errors and uncertainties in the exact location of the anatomy during an intervention. Many methods of compensating for the motion during image reconstruction and therapy delivery have been developed, but these require accurate knowledge of how the internal anatomy is moving, and it is often difficult or impossible to directly measure this motion. Therefore, respiratory motion models have been proposed, which use a correspondence model to relate the motion of the internal anatomy to an easily measured respiratory surrogate signal, such as the height of the patientâŁ™s chest or abdomen. The models are built from synchronised imaging and surrogate data, and can then be used to estimate the motion when just the surrogate data is acquired. Note, the imaging data used to build the models must be acquired fast enough to "freeze" the respiratory motion, whereas the image acquisitions where the models are used to compensate for the motion can be much slower.
First we will give a short overview of our dataset in section 2, followed by section 3 explaining the methods of estimating our model. This includes describing the surrogate signals, correspondence models and its evaluation. In the results section, section 4, we will generate all three surrogate signals we use to fit our models. After fitting all models using the training images we will evaluate the best models with the test images in section 5. After some further analysis of our best model we will look at some computational aspects and finally round of with a discussion and conclusion section in the end of the paper.

2 Dataset

The dataset includes 1500 sagittal cine-MR images, acquired at about 3fps representing a total of 500 seconds of respiration, one example image can be found in figure 1 on the left. The in-slice resolution is $2 \times 2\ mm^2$ and the slice thickness is $10\ mm$. The internal motion has been estimated using B-spline deformable image registration that allows for sliding between two regions, where the first region represents all inner organs including lung and liver and the second region comprising the outer anatomy, such as rib cage and muscles. The deformation of each region is stored as a series of deformations of a regular control point grid (CPG). The boundaries between the regions are given within mask maps.
As the respiratory motion of the lungs mostly arise in the Anterior-Posterior (AP) and Superior-Inferior (SI) directions we use sagittal slices. Looking at figure 1 in the middle plot where the mean of Image 1 and Image 7 is plotted we can see the SI direction pointing up from the target image 1 diaphragm to the source image 7 diaphragm showing the motion from the beginning to the end of one exhalation phase. On the right plot of figure 1 you can find the absolute difference between image 1 and image 7, brighter areas are show bigger difference, therefore perfect areas to place surrogate signals are for instance the skin surface on the abdomen and the chest and on the diaphragm itself.
We are also provided with 1500 registration results, the B-spline transformations, i.e. deformations at the CP locations for each region,

resulting from registering the images. Registration is the mapping from a target to a source image. Within this paper the selected source image used is the first image at exhalation, image 7, as in figure 1 on the left image. Using the registration results we warp the source image 7 to match the reference image, for instance if we assume image 1 to be the target image we can see the registration of it in figure 2 on the left. Its squared residual motion is plotted in the middle of figure 2 and shows the highest residual motion on the skin surface around the chest. One reason for that are not enough control points close to the border of the body masks, in this case outer border of mask 2. In the right plot of figure 2 we see all deformation field arrows on top of the registration of Image 1 pointing from the target image to the source image, in this case from image 1 to image 7.
Most of the provided data is in nifti format, in the form of 5D data, 1^{st} and 2^{nd} dimension of size 160 each containing the sagittal MR image values. The 3^{rd} and 4^{th} dimension are ignored in this paper and are therefore of singular dimension whereas the 5^{th} contains the deformed location of the CP and has size 2. For the sliding registration we are given a signed distance map which determines internally with B-spline transformation to use.
Other provided data we will use include 4 anatomical landmarks, blood vessels in the lungs, automatically tracked using an independent method, used to assess the registrations and motion models, as plotted in figure 1 on the left image. Furthermore a deformation field mask in the source image domain used when calculating the deformation field error to ignore pixels outside the body.

3 Methods

3.1 Surrogate Signal

In this section we explain different physical measurements to be used as surrogate data for respiratory motion models and therefore assume a strong relationship with the true motion model. On top of that we want them to be acquired relatively easily and with sufficiently high temporal resolution.
Within this paper we will focus on scalar surrogate data. The most common signal in MR image acquisition has been the MR navigator echo. Another way of measuring surrogate signals is possible using a spirometer to measure the air flow to and from the lungs, which is commonly used for testing pulmonary function. One other way of acquiring respiratory surrogate data as surrogate signals is tracking the motion of specific points on the surface of the chest or abdomen, which we will measure via image-based signals and are called Anterior-Posterior (AP) direction signals. Surrogate signals measured from the internal anatomy are also commonly used, but are much more challenging to measure during treatment. Using full 2D images of the internal anatomy to generate surrogate data instead is way easier, we will look at the up and down movements of the diaphragm, which therefore is a Superior-Inferior (SI) direction signal. [7, 6]

3.2 Correspondence Models

In this section we will describe different models to relate the internal motion to only one or various respiratory surrogate signals. We will see that separating surrogate signals into inhalation and exhalation will result in better model fitting.

3.2.1 Linear Models

Often used models in the literature are linear correspondence models, which model respiratory motion (m) as a linear combination of surrogate signals s:

$$m = C_0 + C * s \tag{1}$$

where s is a vector of different surrogate signals, i.e. $s = [s_1, s_2, ..., s_N]^T$ with N surrogate signals. C is a $M \times N$ matrix of linear coefficients, and C_0 representing the intercept, a M element vector of constant terms. [6]

3.2.2 Polynomial Models

In contrast to linear models polynomial models estimate the motion as a polynomial function of the surrogate signal(s). In this paper we only have a look at those using a single scalar surrogate signal s_1:

$$m = \sum_{i=0}^{p} C_i s_1^i \tag{2}$$

where p is the order of the polynomial. In this paper we will focus on 2^{nd} and 3^{rd} order polynomials, as higher polynomials normally tend to over-fit the data and lead to very large extrapolation errors. [6]

3.2.3 One surrogate signal

In this part we will only use one surrogate signal to fit a model. Surrogate signals which are easier to measure are all corresponding to skin motion due to breathing. Therefore the first signal we use to relate to the internal motion is the abdominal respiration signal (s_1) which is triggered by the motion of the lungs in the Anterior-Posterior(AP) direction. The correspondence model will relate the deformation as described by the control points to the surrogate signal using the following models:

$$\mathbf{M1} : x = c_0 + c_1 s_1 \tag{3}$$

$$\mathbf{M2} : x = c_0 + c_1 s_1 + c_2 s_1^2 \tag{4}$$

$$\mathbf{M3} : x = c_0 + c_1 s_1 + c_2 s_1^2 + c_3 s_1^3 \tag{5}$$

where M1 is a linear, M2 a 2^{nd} order polynomial and M3 a 3^{rd} order polynomial model. x corresponds to the deformation at each control point and c_n are the model coefficients that need to be fit to the data.

3.2.4 Other surrogate signals

To be able to predict an even better respiratory motion model we add another AP location of the skin surface but now in the chest region (s_2). And a slightly more difficult signal to measure (s_3), as it corresponds to the superior-inferior(SI) location of the diaphragm and we have to use a contour detector to find these points, leading to the following linear models:

$$\mathbf{M4} : x = c_0 + c_1 s_2 \tag{6}$$

$$\mathbf{M5} : x = c_0 + c_1 s_3 \tag{7}$$

$$\mathbf{M6} : x = c_0 + c_1 s_1 + c_2 s_2 + c_3 s_3 \tag{8}$$

3.2.5 Separately modelling inhalation and exhalation

Another way of achieving even better results is to separate all surrogate signals into those corresponding to the inhalation and those to the exhalation phase of the respiration, via derivation. After splitting these signals we will model two independent models on both signals:

$$\mathbf{M7} : x_{inhalation} = c_0 + c_1 * s_{1_{inh}} \tag{9}$$

$$x_{exhalation} = c_0 + c_1 * s_{1_{exh}} \tag{10}$$

$$\mathbf{M8} : x_{inhalation} = c_0 + c_1 * s_{2_{inh}} \tag{11}$$

$$x_{exhalation} = c_0 + c_1 * s_{2_{exh}} \tag{12}$$

$$\mathbf{M9} : x_{inhalation} = c_0 + c_1 * s_{3_{inh}} \tag{13}$$

$$x_{exhalation} = c_0 + c_1 * s_{3_{exh}} \tag{14}$$

which will lead to better overall results looking at the combination of these two models. [7]
When we also include all other signals we can get even better results, as can be seen in the results section, where we train all different models and test those with the best training results in more depth.

3.3 Evaluation

After training our models on a specific training set we test and evaluate the fitted motion models using the remaining images as a test set. We therefore will use the best models within our training data and try to evaluate their performance on the test set. First we will derive model selection values as AIC and BIC for the train and test set to get the best model. To evaluate this model in more depth we use the following three techniques to assess the model estimates: Visual Assessment, Deformation Field Error and Landmark Error. On top of that we will estimate the uncertainty in the models using the standard bootstrapping method.

3.3.1 Model Selection

Various statistics can be used to measure the quality of a model. These include the Akaike information criterion (AIC), Bayesian information

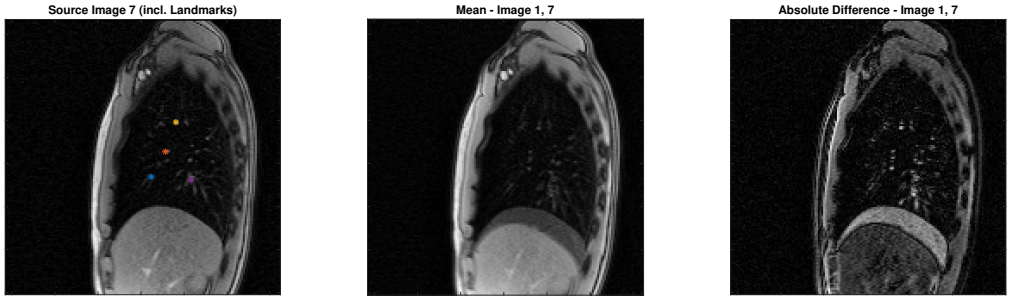

Fig. 1: Dataset Example

Fig. 2: Image 1 Registration

criterion (BIC) and a lot more, which we do not cover in this paper. We will also look at the sum of squared errors (SSE), although we can only use it to compare models having the same number of variables. Because the training error will decrease as more variables are included in the model, but the test error may not. So the SSE cannot be used to select models among different numbers of variables. [2]
Taking the general assumption of Gaussian noise of general linear regression models into account, we have the following AIC:

$$AIC = 2 * N + K * log(K^{-1} * \sum_{k=1}^{K}(A_k - S_k)^2) \quad (15)$$

where N is the number of parameters in the model, including the intercept and the unknown variance which is also estimated. K is the sample size and

$$SSE = \sum_{k=1}^{K}(A_k - S_k)^2 \quad (16)$$

is the sum of squared errors of a model, A_k being the true value and S_k the estimated value. As of the loss is logarithmic the AIC procedure takes the model which minimizes the value in equation 15. It is clear that more complex models (with larger N) will suffer from larger penalties.
Whereas the BIC is slightly different, which is another popular model selection principle, selecting the model that minimizes:

$$BIC = N * log(K) + K * log(K^{-1} * \sum_{k=1}^{K}(A_k - S_k)^2) \quad (17)$$

The only difference between AIC and BIC is that the constant in the penalty term of AIC is replaced with the logarithm of the sample size to get its BIC value. [1]

3.3.2 Visual Assessment

We are using the transformations estimated by the models to deform the test images and display the deformed images. If the motion was estimated perfectly the deformed source image would exactly look like the target image.

3.3.3 Deformation Field Error

In this section we derive the difference of the deformation field resulting from our estimated transformation and the deformation field resulting from the registration result for the target image. We only look at pixels within the deformation field mask and calculate the L2 norm of the deformation field errors. Since the mask is defined in the source image space we have to transform it using the registration. We will repeat this for each image.

3.3.4 Landmark Error

Another possible evaluation can be done by using the landmark locations. We therefore calculate the difference between landmark locations estimated by the model and those provided in the data file. To calculate the landmark locations estimated by the model we have to transform the landmark locations from the target images into the space of each source image, using the model estimated transform. After that we calculate the landmark error for each landmark and each test image.

3.4 Estimating the uncertainty in the models

To estimate the distribution of the model parameters we use the standard bootstrapping method as follows:

$$\hat{A}_{tk} = A_{\lfloor U(1,K+1) \rfloor} \quad (18)$$

where A_k are the true values of the parameters and the subscript on the right hand side is a uniformly distributed integer in the range 1,...,K.

4 Results

4.1 Generate the surrogate signals

We generate the following three surrogate signals, plotted in figure 3:

- **Abdominal signal**: Finding the AP location of the skin surface at y=150 pixels in each image. Therefore we want to find the first point in the image corresponding to an intensity of 20 when coming from the anterior (x=0) side of the image. Linear interpolation was used to estimate this point to sub-pixel accuracy. You can find the this point of image 1 in figure 3 showed by the blue point in the left plot and the blue line on the right plot shows this signal for the first 100 images, centered around zero via subtraction of its mean value, to make it comparable with the other signals. The peaks correspond to the end of exhalation and the throughs to the end of inhalation.
- **Chest signal**: Finding the AP location of the skin surface at y=50 pixels in each image. Again we want to find the first point in the image corresponding to an intensity of 20 when coming from the anterior (x=0) side of the image including linear interpolation to get sub-pixel accuracy. You can find this point at image 1 in figure 3 showed by the red point in the left plot and the red line on the right plot shows this signal for the first 100 images, again centered around zero.
- **Diaphragm signal**: Finding the SI location of the diaphragm at x=87 pixels in each image. Therefore we used the matlab function imcontour() to find all contour lines of each image, plotted in figure 3 in the middle plot for image 1, and then we take the most inferior contour. You can find this point of image 1 in figure 3 showed by the yellow point in the left plot and the yellow line on the right plot shows this signal for the first 100 images centered around zero. In this case the peaks correspond to the end of inhalation and the throughs to the end of exhalation.

Looking at the right plot in figure 3 we see that although the skin surface surrogate signals are easily measured the output is not that good. Whereas the abdominal surrogate signal represents a signal corresponding to the respiratory motion including some noise at the peaks and throughs of the line, the chest surrogate signal is a lot worse and a lot noisier. In contrast if we look at the diaphragm surrogate signal we can see a solid plot including concrete peaks and throughs without much noise. To get an even better analysis of that we looked at the inhalation and exhalation part of all surrogate signals according to their gradient as can be seen in figure 4. We can see that both surrogate signals derived at the skin surface show noise, especially the abdominal signal in peak regions. Summing up all changes from inhalation to exhalation and vice-versa we get a total of 38 and 37 for chest and abdominal surrogate signal respectively and only 27 looking at the diaphragm surrogate signal, which estimates only one false inhalation and exhalation around image 58, so we expect to achieve better results using this signal to estimate our model.

4.2 Fitting Models

As a first step we will now fit the models using 100 registration results and then assess the results with the remaining 1400, the results can be found in table 1. For instance looking at CP 44,38 of region 1 we estimate a linear model (M1), 2^{nd} order polynomial (M2) and 3^{rd} order polynomial model (M3) and show the results in figure 5. The corresponding residual fitting error of these CP deformations are 328.75, 325.27 and 271.62 respectively. Looking at their one pixel AIC model M1 has a lower value than model M2, but model M3 is the best, same order looking at the BIC. If we take all pixels into account we can see that the AIC is similar for all three models, but the lowest BIC has model M1. Therefore we do not look at model M2 and M3 any more.

If we now separate the model into two models, one fitting the inhalation data and the other the exhalation data we get the results as can be seen in figure 6. As expected, both models M7(Inh) and M7(Exh) are different from the full model M1 and we achieve an overall better result reducing the SSE from 2.72e+06 of model M1 to 2.57e+06, which is the sum of the inhalation and exhalation model SSE.
Using the second surrogate signal measured at the chest (s2) and applying linear model M4 we can see its results plotted in figure 7. As expected we do not get a gaussian distributed surrogate value within our data points, but we have values concentrated around a surrogate value of about 60.1 to 60.5 with some possible outliers around 59.5 and one obvious outlier at 58.7. Our model overweighs the outliers in our data and therefore we get a very high SSE, which is the highest over all models we are looking at, with 4.85e+06 SSE including all pixels. Separating it into two models, M8(Inh) and M8(Exh), does not change that much and still is one of the worst fittings.
Whereas looking at our surrogate signal measuring respiratory motion on the diaphragm we see a very good fit even looking at the linear model M5, with one of the lowest SSE values overall, 2.46e+06. In this case separating the model into the inhalation and exhalation part slightly decreases its SSE

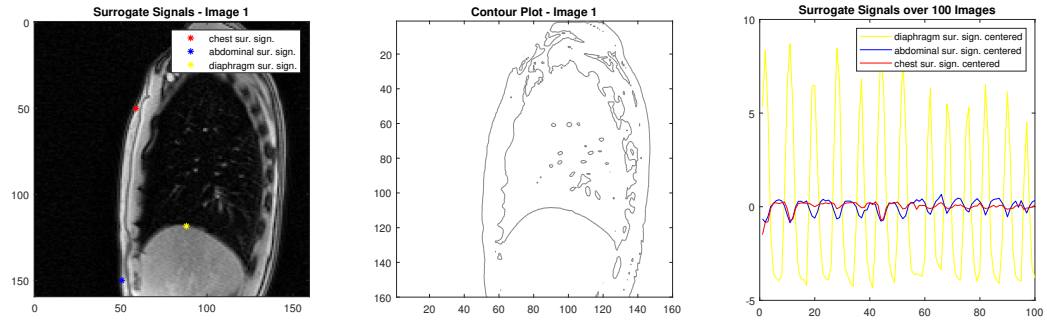

Fig. 3: Surrogate Signals

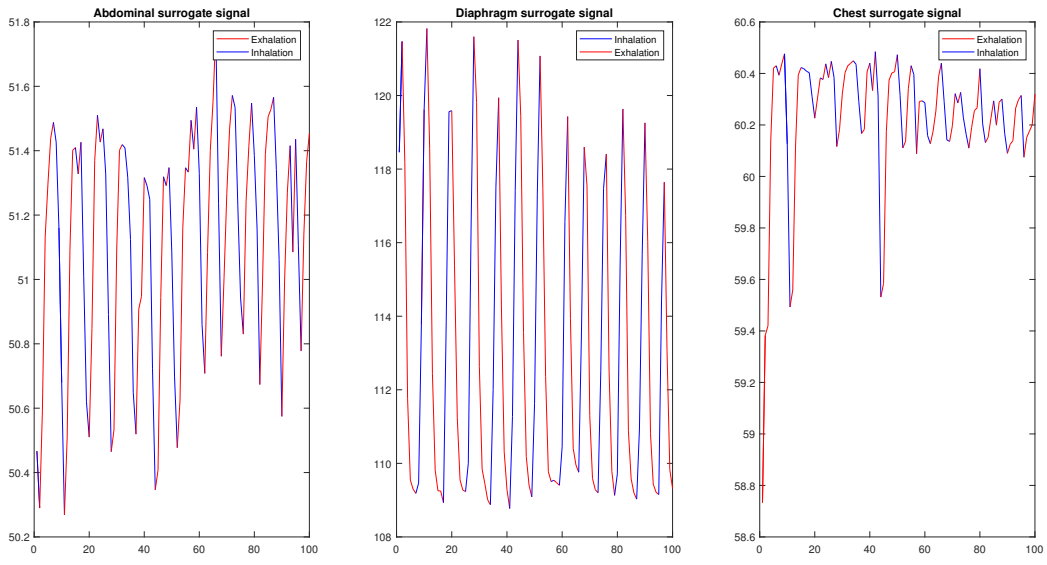

Fig. 4: Surrogate Signals - Gradients (Inhalation and Exhalation)

to 2.38e+06 as well as its AIC and BIC. Its BIC value over all pixels is the lowest throughout all different models.
Another very good model we found is model M6, which includes all different surrogate signals and has the lowest SSE and AIC if including all pixels.
So we can say that model M6 and M9 fit the data best in the training data. Now we have to find out if this is the case looking at the test data, the remaining 1400 images, to validate the fitting. Therefore we will look at the 3 best models considering the training fit, which are model M5, M6 and M9 and we include our initial model M1 as a base line in the following section.

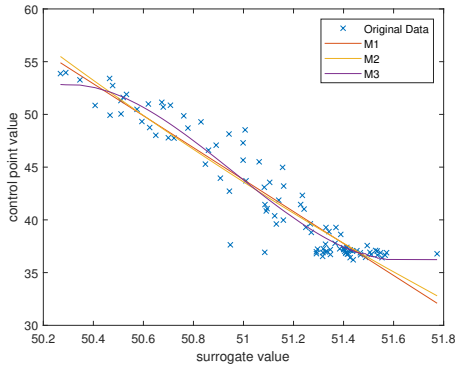

Fig. 5: Abdominal surrogate signal - Linear, quadratic, cubic

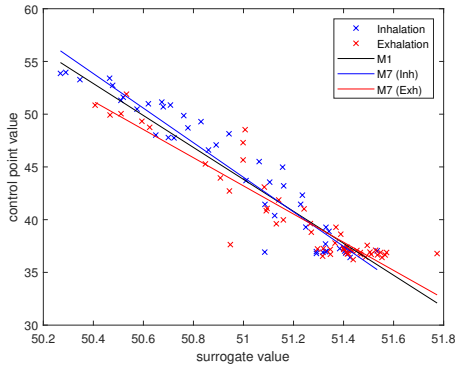

Fig. 6: Abdominal surrogate signal - total and separated

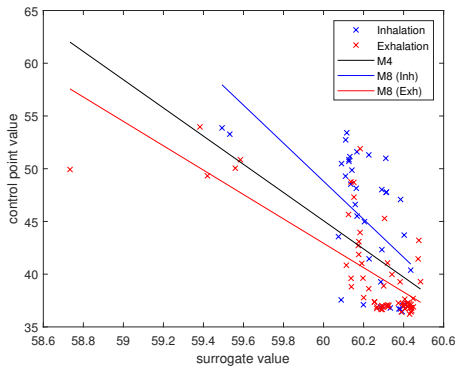

Fig. 7: Chest surrogate signal - total and separated

5 Evaluation

Now we are going to test our trained models M1, M5, M6 and M9 with images 101 to 1500, so the remaining 1400 images.

5.1 Model Selection

Calculating SSE, AIC and BIC again, now using all test images, we get the lowest value for all three measurements using model M9. As in table 2 mentioned model M9 has the lowest values for all three measurements with 3.37e+07, 7.51e+06 and 8.32e+06 as SSE, AIC and BIC respectively. Therefore we take model M9 as our best model and will have a look into the evaluation details in the following sections.

5.1.1 Visual Assessment

The first technique to assess the model estimates is the visual assessment. In figure 9 we can find the registration in the top right plot and the model M9 estimates with target image 101 in the top left. Looking at the images and estimations we cannot really see a big difference. But looking at the residual motion, bottom right plot of figure 9, we see a slightly less appropriate estimation using our model M9 compared to the registration model. In the bottom left plot of this figure the sum of residuals of each image was derived and plotted. We can see a slight increase of the residual sum of Model M9 in later images, whereas the residual sum of the registration model rather stays at the same level over all images. Though one conspicuous pattern can be seen in the plot, little jumps at specific images. The first spike is at image 113. Therefore we have taken a look at this specific image in figure 10 where we can see the rather worse estimation. But the same pattern can be found looking at the registration results of this specific image.

5.1.2 Deformation Field Error

In this section we derive the difference between the deformation field resulting from our estimated transformation and the one resulting from the registration result for the target image. The difference of both models will be evaluated using L2 Norm and can be seen in figure 11, where we see the same pattern as in the visual assessment, that model M9 is estimating later images worse than the registration model. We also plotted the mean L2 Norms of every pixel to get a mean L2 Norm image to be able to see the areas where our model has bigger problems (brighter areas), as you see in figure 12. The worst estimation of our model compared to registration

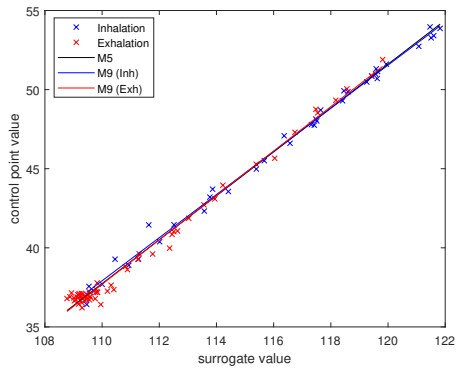

Fig. 8: Diaphragm surrogate signal - total and separated

	SSE(43,38)	SSE(all)	N (if all *17956)	K (if all *17956)	AIC(43,38)	AIC(all)	BIC(43,38)	BIC(all)
M1	328.75	2,720,000	3	100	125.01	8.53e+05	132.83	1.52e+06
M2	325.27	2,670,000	4	100	125.95	8.56e+05	136.37	1.75e+06
M3	271.62	2,550,000	5	100	109.92	8.09e+05	122.95	1.92e+06
M4	2,030	4,850,000	3	100	307.06	1.89e+06	314.88	2.56e+06
M5	17.66	2,460,000	3	100	-167.39	6.73e+05	-159.57	1.34e+06
M6	16.57	2,120,000	5	100	-169.76	4.78e+05	-156.73	1.59e+06
M7-Inh	141.03	1,340,000	3	46	57.54	5.07e+05	63.02	1.13e+06
M7-Exh	156.67	1,230,000	3	54	63.52	3.38e+05	69.49	9.73e+05
M7 (SSE Sum)	297.7	2,570,000	3	100	115.09	7.52e+05	122.91	1.42e+06
M1	328.75	2,720,000	3	100	125.01	8.53e+05	132.83	1.52e+06
M8-Inh	872.72	2,180,000	3	38	125.09	9.00e+05	130.01	1.52e+06
M8-Exh	626.9	1,980,000	3	62	149.45	7.49e+05	155.83	1.39e+06
M8 (SSE Sum)	1,499.62	4,160,000	3	100	276.78	1.62e+06	284.60	2.28e+06
M4	2,030	4,850,000	3	100	307.06	1.89e+06	314.88	2.56e+06
M9-Inh	5.7	1,000,000	3	38	-66.09	3.69e+05	-61.18	9.84e+05
M9-Exh	11.44	1,380,000	3	62	-98.78	3.47e+05	-92.40	9.89e+05
M9 (SSE Sum)	17.14	2,380,000	3	100	-170.38	6.14e+05	-162.56	1.28e+06
M5	17.66	2,460,000	3	100	-167.39	6.73e+05	-159.57	1.34e+06

Table 1. Training Set - Model Selection - SSE, AIC, BIC

	SSE(train)	AIC(train)	BIC(train)	SSE(test)	AIC(test)	BIC(test)
M1	2.72e+06	8.53e+05	1.52e+06	7.00e+07	2.59e+07	2.67e+07
M5	2.46e+06	6.73e+05	1.34e+06	3.43e+07	7.95e+06	8.76e+06
M6	2.12e+06	4.78e+05	1.59e+06	4.07e+07	1.23e+07	1.37e+07
M9	2.38e+06	6.14e+05	1.28e+06	3.37e+07	7.51e+06	8.32e+06

Table 2. Test Set - Model Selection - SSE, AIC, BIC

can be identified in the lower right boundary between region 1 and region 2, which is the posterior region of the diaphragm.

5.1.3 Landmark Error

Finally we look at the difference between landmark locations estimated by the model and those provided by the data. In this section we calculated the landmark error for each landmark and each test image and plotted the average L2 Norm of all 4 Landmarks for every test image in figure 13. In this case the increasing pattern is not that obvious so we plotted a moving average of the last 100 images on top of that, to be able to see the same pattern of increasing L2 Norms at later images. In figure 14 we plotted the L2 Norm for all landmarks and all test images. On the left plot we see the 4 Landmarks of the Source Image 7, where Landmark 1 is the bottom left blue dot, Landmark 2 the middle red one, Landmark 3 the yellow top

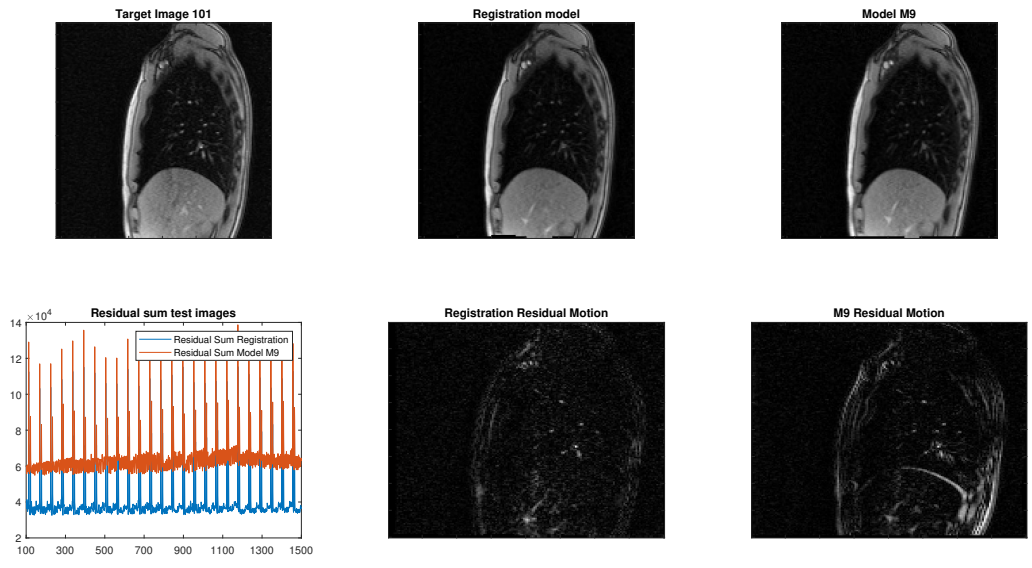

Fig. 9: Visual Assessment - Comparing Residual Motion of Registration and Model M9 for image 101 and all images

one and Landmark 4 the bottom right one. Looking at the right plot we can see bigger errors for Landmark 4 and Landmark 1 as expected, as they are moving a lot more during respiratory motion lying in more inferior regions of the lung than the others. The most superior one is Landmark 3 and therefore has the lowest error as it does not move that much. The average error of each Landmark over all 1400 test images is as follows:

- Landmark 1: 2.59
- Landmark 2: 2.09
- Landmark 3: 1.62
- Landmark 4: 3.18

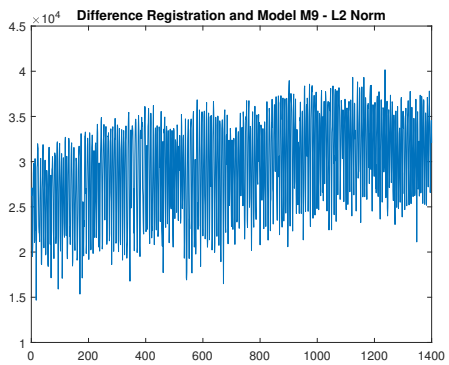

Fig. 11: Deformation Field Error - L2 Norm sum of every test image

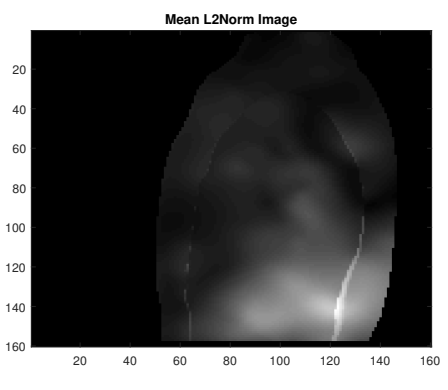

Fig. 12: Deformation Field Error - Mean L2 Norm Image of all test images

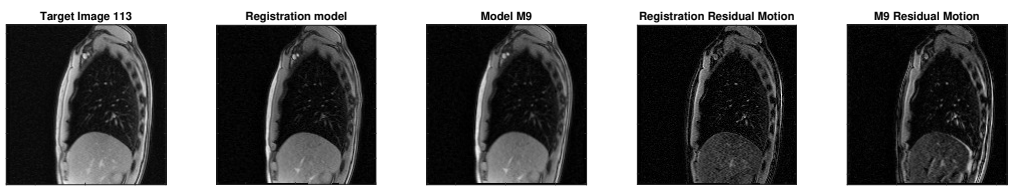

Fig. 10: Visual Assessment - Residual Motion of both models for outlier test image 113

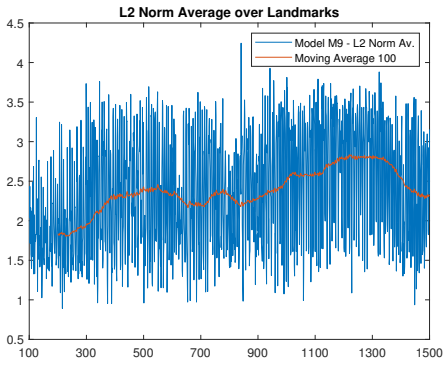

Fig. 13: Landmark Error - L2 Norm Average over all 4 Landmarks for all 1400 test images

5.1.4 Comparing three assessment procedures

Comparing all three methods of assessing the model we can say that visual assessment is rather an easy way of analysing the model results and is straightforward. Whereas looking at the Deformation field error and at the Landmark error we get a more specific evaluation of our model results which are better interpretable. In general we see an overall agreement of all three methods having a trend to achieve worse results looking at later test images. Therefore as our general result we can say that model M9 fits the data pretty well and is getting reasonably close results compared to the benchmark registration model.

5.2 Computational time varies over different fitting methods

We also looked at the computational time of different matlab implementations of the model fitting, using *pinv*, the *mldivide ( )* operator and *lsqminnorm ()*.

The mldivide operator solves a system of linear equations, for instance $x = A\backslash B$ solves $A * x = B$. *'pinv'* instead returns the Moore-Penrose Pseudoinverse of a matrix. For a any matrix A the pseudoinverse exists and is unique. If A is square and not singular pinv(A)=inv(A). However, if A is not square or if it is square and not singular, then inv(A) does not exist but pinv(A) satisfying all of the following conditions:

$$ABA = A \tag{19}$$

$$BAB = B \tag{20}$$

$$(AB)^* = AB(AB\ Hermitian) \tag{21}$$

$$(BA)^* = BA(BA\ Hermitian) \tag{22}$$

The computation is based on svd(A) and singular values less than a specific tol value are treated as zero. [4]

The results differ, as pinv returns a solution with minimum norm, while mldivide returns a solution with at most rank(A) nonzero components. [5] lsqminorm() is similar to pinv returning a solution with minimal norm, but is generally more efficient than pinv, and it also supports sparse matrices. [3]

The computational time differs sligthly between the three methods when deriving model M1. Doing so for an entire number of 100 times and taking the mean computational time, pinv is the fastest with 0.0077 seconds, then mldivide with 0.0372 seconds and lsqminorm is slowest with 0.0378 seconds of computational time.

6 Discussion and Conclusion

Overall, we found a model fitting the data pretty well, although there are ways of possibly finding even better ones which we will describe in the next paragraph.

One possibility is to validate models using K-Fold Cross Validation, which cuts the whole dataset K times into training and test data. The idea is to split up the data into K subsets of approximately equal size. These K different training and test sets will be carried out using (K-1) subsets to train the model on and the remaining one to test it. The final comparable measure is the mean over all obtained performances. As a result we would also come up with the general idea of having more training data than test data. Although we have to take care about overfitting and should look at the training and test results in more detail. Another way of trying to get a better model fit is to use more surrogate signals in the model. Again we should care about the test fit, as we easily could overfit using to many surrogate signals in our model. One specific surrogate signal we would suggest using might be one at the posterior part of the diaphragm, which is the are we saw the most error in our model. In further research methods we would also try to fit different correspondence models and might use more machine learning related, advanced methods as for example oftenly used in Deep Learning: LSTMs, for example.

Code: https://www.dropbox.com/sh/3mnnv2tbfhj2osz/AACwJVHgyFSD0zqmCfK0Cq5va?dl=0

References

[1]J. Ding, V. Tarokh, and Y. Yang. Model selection techniques - an overview. *IEEE Signal Processing Magazine*, 2018.

[2]G. James, D. Witten, T. Hastie, and R. Tibshirani. *An Introduction to Statistical Learning: With Applications in R*. Springer Publishing Company, Incorporated, 2014.

[3]MathWorks. lsqminnorm, 2019.

[4]MathWorks. mldivde, 2019.

[5]MathWorks. pinv (moore-penrose pseudoinverse), 2019.

[6]Jamie McClelland. *Estimating Internal Respiratory Motion from Respiratory Surrogate Signals Using Correspondence Models*, pp. 187–213. 05 2013.

[7]J.R. McClelland, D.J. Hawkes, T. Schaeffter, and A.P. King. Respiratory motion models: A review. *Medical Image Analysis*, 17(1):19–42, 2013.

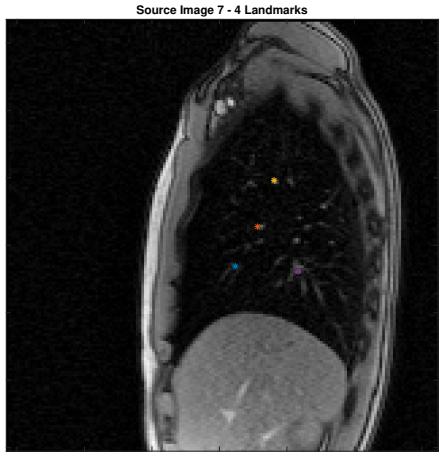

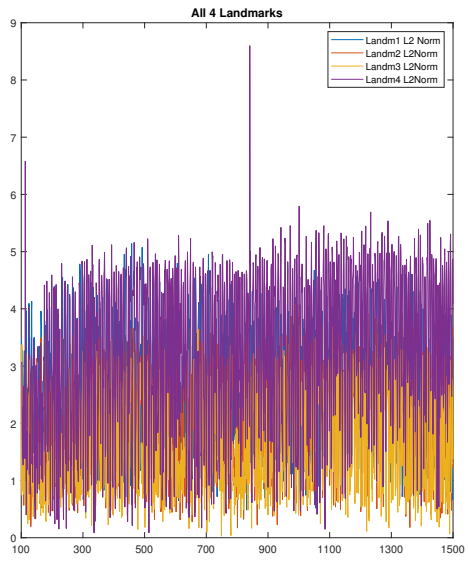

Fig. 14: Landmark Error - L2 Norm of all 4 Landmarks